doi:10.6041/j.issn.1000-1298.2016.07.050

Multiphase Flow Detection Based on ECT Image Reconstruction Algorithm

Zhao Yulei Guo Baolong

(*School of Aerospace Science and Technology*, *Xidian University*, *Xi'an* 710071, *China*)

Abstract: Although Landweber method is a classical algorithm for image reconstruction in electrical capacitance tomography (ECT) system, the application of Landweber method in multiphase flow detection is limited due to its semi-convergence. To solve this problem, this paper analyzed and proved the semi-convergence of Landweber method mathematically so as to explore its physical properties. Based on this, an improved Landweber method with full and stable convergence was proposed by structuring a compression operator for Landweber. Then the "soft field" characteristic of sensitivity field in ECT sensor and its effect on sensitivity distribution, which is an important basis for image reconstruction, were analyzed. The sensitivity distributions for each typical electrode pair under different flow patterns were given in three-dimensional graphics. As ignoring "soft field" characteristic leads to inconsistency of the best iteration times of Landweber for different flow regimes, an adaptive iteration stopping criterion was proposed. The criterion is based on a priori condition obtained by training a number of image samples with least square support vector machine. With this criterion, iteration can be stopped when the image reconstructed is the closest to the actual distribution of multiphase flow. Meanwhile, the effect of "soft field" characteristic on image reconstruction could be compensated. The experimental results prove that the method not only has a stable convergence, but also can improve the image accuracy by 16% ~ 50%. Therefore, the full-convergence Landweber method can be widely used in none real-time multiphase flow measurement and detection system for its high detection precision.

Key words: multiphase flow; detection; image reconstruction; electrical capacitance tomography; Landweber method

0 Introduction

In agricultural production, the detection of multiphase flow is needed frequently. For example, it is needed to detect the moisture content of wheat and corn, split-phase holdup of milk, soil salinity, and food[1]. Another example is the non-destructive testing of the oil pipeline in agricultural machinery. Electrical capacitance tomography (ECT) is a multiphase flow density measurement and visualizing monitoring technology which is regarded as one of the most promising process tomography technology for being non-invasive, rapid, and low-cost and non-radioactive[2-4].

Image reconstruction algorithm is critical in the successful application of ECT technology. Especially for the multiphase flow in the agricultural production, the accuracy of image reconstruction plays an important role in the test results[5]. Currently, ECT image reconstruction can be realized by linear back-projection (LBP) algorithm[6], Landweber iteration[7], Tikhonov regularization[8], Newton-Raphson method, conjugate gradient (CG)[9] and so on.

Among the methods mentioned above, LBP and Landweber method are comparatively mature and the most widely used ECT image reconstruction algorithms[10]. LBP is quick and easy to use, but with poor image quality. Strictly speaking, it's only a qualitative algorithm[4,10]. Landweber is the most classic image reconstruction iteration algorithm which enjoys the iconic status in ECT image reconstruction[11]. From the perspective of optimization, Landweber iteration approximates error minimization function through the linear function in the steepest descent direction based on the steepest descent principle. However, in the application of Landweber

Received date: 2016-01-03 Accepted date: 2016-03-13

Supported by National Natural Science Foundation of China (Grant Nos. 61571346, 61305041, 61305040), Fundamental Research Funds for Central Universities (Grant No. JB1401305)

Corresponding author: Guo Baolong, Professor. E-mail: blguo@xidian.edu.cn. Tel: +86-029-88202249

method, with the increase of the number of iterations, the reconstructed image sequence may become divergent (semi-convergent) after a period of convergence[12]. One of the reasons is that the ECT sensor sensitivity field is nonlinear and has soft field characteristics; the other is that the number of independent projection data of capacitance sensor (the number of independent capacitance) is less than the pixel number of the reconstructed images[13-14]. In addition, for different flow regimes, the numbers of iterations with Landweber method are inconsistent, which makes it hard to establish a criterion for stopping iteration. Therefore, on the basis of Landweber method, if an improved method can be proposed, which is able to solve semi-convergence and compensate the influence of "soft field" characteristic, it will be significant for the application of ECT in agricultural machinery.

To address the problem of semi-convergence of Landweber image reconstruction, the soft field characteristics of the ECT sensitivity field and the effects of sensitivity matrix of ECT sensitivity field on the image reconstruction algorithm were analyzed, then the semi-convergence of Landweber method was demonstrated and its reasons are explored. A new method to improve the iterative operators of Landweber method and the criterion to stop iteration was proposed to realize fast and stable convergence of the reconstructed image. At last, the image reconstruction experiments of the new method were performed, and the results were compared with those of Landweber method.

1 Analysis of ECT sensitivity field characteristic and imaging principle

1.1 Basic principle of ECT

Each phase separation medium of the multiphase fluid in the pipeline has a different permittivity. When the phase concentration and distribution of the fluid change, the equivalent permittivity of the multiphase flow will also change. So the measuring capacitance values between the electrodes pair will be changing too[10]. Measurements of the changes in capacitance between a set of electrodes, which are placed around the periphery of a subject, are made. These measurements form a set of projections. With a proper image reconstruction algorithm, an image of the cross-sectional distribution of dielectric materials within the subject can be reconstructed from the measured data.

A typical ECT system as shown in Fig. 1 comprises three main units: a multi-electrode sensor, measurement and data acquisition, and a computer for image reconstruction.

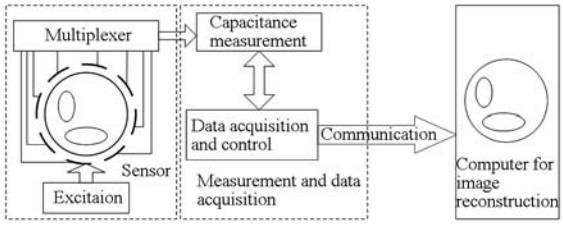

Fig. 1 Compostion structure of ECT system

As the excitation frequency is about 1kHz, there is no free electron in the sensor, and sensitivity field can be regarded as electrostatic field. So the field in the sensor can be described with Possion equation as

$$\nabla(\varepsilon(x,y)\ \nabla\phi(x,y))=0 \tag{1}$$

where, $\varepsilon(x,y)$ is the permittivity distribution in the section of pipeline, $\phi(x,y)$ is the potential distribution, ∇ is the gradient operator.

After exerting boundary condition, the relationship between capacitance and permittivity distribution is governed by the following equation:

$$C=\frac{Q}{V}=-\frac{1}{V}\iint_{\Gamma}\varepsilon(x,y)\ \nabla\phi(x,y)\,\mathrm{d}\Gamma \tag{2}$$

where, Q is the charge in the electrode to the capacitance C, V is the potential difference between two electrodes forming the capacitance, Γ is the electrode surface.

By introducing a sensitivity field function $S(x,y,\varepsilon(x,y))$, we can describe the relationship of capacitance C and $\varepsilon(x,y)$ as

$$C=\iint_{D}\varepsilon(x,y)S(x,y,\varepsilon(x,y))\,\mathrm{d}x\mathrm{d}y \tag{3}$$

To simplify the equation, the soft field effect is usually ignored, that is to say, assume that the sensitivity field function is irrelevant to $\varepsilon(x,y)$, and then Eq. (3) can be discretized, linearized and normalized as

$$\boldsymbol{\lambda}=\boldsymbol{S}\cdot\boldsymbol{g} \tag{4}$$

Where, $\boldsymbol{\lambda}\in\mathbf{R}^m$ is the normalized capacitance vector; $\boldsymbol{S}\in\mathbf{R}^{m\times n}$ is the normalized sensitivity matrix; $\boldsymbol{g}\in\mathbf{R}^n$ is the normalized permittivity vector, namely the medium distribution vector[15].

The image reconstruction of ECT is to obtain the

permittivity distribution by the measured capacitance, i. e. to solve the unknown $\boldsymbol{\lambda}$ from the known amount $\boldsymbol{g}$. However, due to the case that the number of known amount is much larger than that of equations, Eq. (4) is indeterminate equation, and the solution of the equation is not unique. Meanwhile, due to the "soft field" characteristic of ECT sensor, there is great impact on image reconstruction. Moreover, Eq. (4) is also a ill-conditioned equation, and the solution is unstable. Therefore, an algorithm of ECT image reconstruction which can solve the above problems is much important.

1.2 "Soft field" characteristic of ECT

Different from the hard field of X-ray and γ-ray, the sensitivity field of ECT sensor is a soft field. The so-called "soft field" mainly refers to the inhomogeneity of the sensitivity distribution. The sensitivity distribution is affected by the medium distribution and the permittivity difference of abnormal medium. "Soft field" characteristic is caused by the polarization of dielectric in electrostatic field. The bound charge can be generated by dielectric under the influence of polarization, and the original electrostatic field will be changed by the electrostatic field generated by the bound charge.

Under the influence of "soft field" characteristic, corresponding to the different dielectric and its distribution, sensitivity distribution has great differences. In the condition that medium distribution is unknown, the distribution is also unknown, so only the sensitivity distribution in the empty field can be used to reconstruct image. This has a great impact on image reconstruction.

The sensitivity distribution characteristics of ECT sensitivity field is illustrated with the empty field, bubble flow, ring flow and layer flow (the medium is gasoline) of an 8-electrode ECT sensor. Electrode-1 is defined as the exciting electrode, while the remaining electrodes are marked in sequence as electrode-2 ~ 8. The sensitivity distribution of all the electrode pairs are shown in Tab. 1. It is seen from the table that the sensitivity distributions of the same electrode pairs under different flow regimes vary a lot. Since sensitivity is the comprehensive reflection of electrostatic field distribution, different flow regimes (even different mediums) will pose a direct effect on the electrostatic field distribution, thus the image reconstruction result is affected.

Tab. 1 Sensitivity distribution under different flow regimes

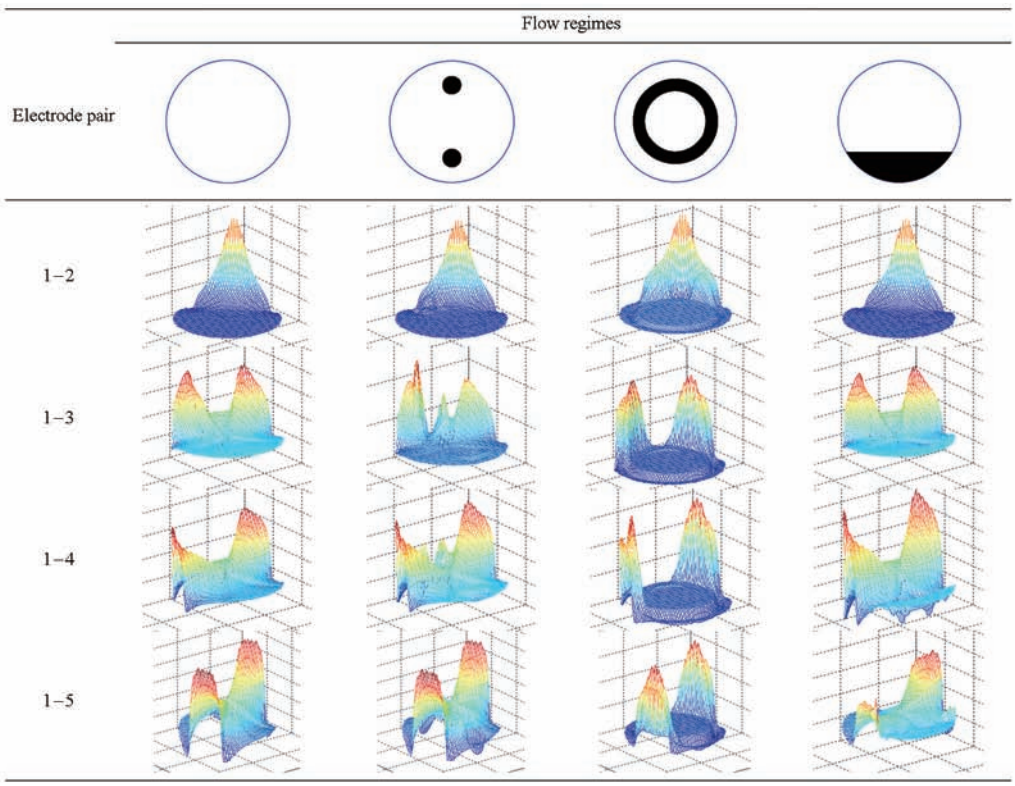

2 Demonstration and analysis of semi-convergence of Landweber method

2.1 Demonstration of semi-convergence of Landweber method

Although Landweber method is the most sophisticated algorithm for ECT image reconstruction currently, the main drawback of this method is semi-convergence, which limits the further promotion of Landweber. In principle, Landweber method is a variation of steepest descent method. To prove the semi-convergence of Landweber method, a deduction is done based on series theory. Actually, the proposer of Landweber method used in ECT image reconstruction also explains the method mathematically with series theory.

For the linear matrix shown in Eq. (4), assume that $\boldsymbol{A}_0$ is the initial approximation matrix of $\boldsymbol{S}^{-1}$, let $\boldsymbol{I}$ be a unit matrix, the residual matrix will be

$$\boldsymbol{R}=\boldsymbol{I}-\boldsymbol{A}_0\boldsymbol{S} \tag{5}$$

If $\boldsymbol{S}^{-1}$ exists, Eq. (5) can be modified as

$$\boldsymbol{S}^{-1}=(\boldsymbol{I}-\boldsymbol{R})^{-1}\boldsymbol{A}_0 \tag{6}$$

If the spectral radius of the residual $\boldsymbol{R}$, that is $\rho(\boldsymbol{R})<1$, $(\boldsymbol{I}-\boldsymbol{R})^{-1}$ sequence could be expanded, and the k^{th} sequence of $\boldsymbol{S}^{-1}$, $\boldsymbol{A}_k$ the $k^{\text{th}+1}$ sequence of $\boldsymbol{S}^{-1}$, $\boldsymbol{A}_{k+1}$ are represented respectively as

$$\boldsymbol{A}_k=(\boldsymbol{I}+\boldsymbol{R}+\cdots+\boldsymbol{R}^{k-1})\boldsymbol{A}_0 \tag{7}$$

$$\boldsymbol{A}_{k+1}=(\boldsymbol{I}+\boldsymbol{R}+\cdots+\boldsymbol{R}^{k})\boldsymbol{A}_0 \tag{8}$$

And as

$$(\boldsymbol{I}-\boldsymbol{R})(\boldsymbol{I}+\boldsymbol{R}+\cdots+\boldsymbol{R}^{k-1})=\boldsymbol{I}-\boldsymbol{R}^k \tag{9}$$

according to Eqs. (5), (7) and (9), the following equation can be obtained.

$$\boldsymbol{R}^k\boldsymbol{A}_0=\boldsymbol{A}_0(\boldsymbol{I}-\boldsymbol{S}\boldsymbol{A}_k) \tag{10}$$

Substitute $\boldsymbol{S}^{-1}$ with $\boldsymbol{A}_{k+1}$, according to Eq. (8), the following equation holds up

$$\boldsymbol{g}_{k+1}=\boldsymbol{g}_k+\boldsymbol{R}^k\boldsymbol{A}_0\boldsymbol{\lambda} \tag{11}$$

Put Eq. (10) into Eq. (11), then

$$\boldsymbol{g}_{k+1}=\boldsymbol{g}_k+\boldsymbol{A}_0(\boldsymbol{\lambda}-\boldsymbol{S}\boldsymbol{g}_k) \tag{12}$$

Let $\boldsymbol{A}_0=\alpha\boldsymbol{S}^{\mathrm{T}}$, then Eq. (12) can be rewritten as

$$\boldsymbol{g}_{k+1}=\boldsymbol{g}_k+\alpha\boldsymbol{S}^{\mathrm{T}}(\boldsymbol{\lambda}-\boldsymbol{S}\boldsymbol{g}_k) \tag{13}$$

where, α is the gain factor, which is used to control the convergence rate.

Eq. (13) is the general iterative equation of Landweber method.

As described above, only when the spectral radius of residual is less than 1, i. e. $\rho(\boldsymbol{R})<1$, Eq. (13) is valid, namely the sequence is convergent. Therefore, according to the series theory, the full convergence condition of Landweber method is $\rho(\boldsymbol{R})=\|\boldsymbol{R}\|_2<1$, and the norm of Operator $\boldsymbol{R}$ can be defined as

$$\|\boldsymbol{R}\|=\max\frac{\|\boldsymbol{R}\boldsymbol{g}\|}{\|\boldsymbol{g}\|}\ (\forall\boldsymbol{g}\in\mathbf{R}^n,\ \text{and}\ \boldsymbol{g}\neq0) \tag{14}$$

Assume that $\boldsymbol{g}=\boldsymbol{x}-\boldsymbol{y},\boldsymbol{x},\boldsymbol{y}\in\mathbf{R}^n$ and $\boldsymbol{x}\neq\boldsymbol{y}$, then

$$\|\boldsymbol{R}\|\geqslant\frac{\|\boldsymbol{R}(\boldsymbol{x}-\boldsymbol{y})\|}{\|\boldsymbol{x}-\boldsymbol{y}\|} \tag{15}$$

Namely,

$$\|\boldsymbol{R}\boldsymbol{x}-\boldsymbol{R}\boldsymbol{y}\|\leqslant\|\boldsymbol{R}\|\cdot\|\boldsymbol{x}-\boldsymbol{y}\| \tag{16}$$

If $\|\boldsymbol{R}\|<1$, then $\boldsymbol{R}$ is the compression operator, it is fully convergent, so the full-convergence condition of Landweber method is that $\boldsymbol{R}$ be the compression operator.

Take 2-norm as an example to discuss the characteristics of $\|\boldsymbol{R}\|$. According to Eq. (5) and the mathematical definition of 2-norm,

$$\|\boldsymbol{R}\|_2=\|\boldsymbol{I}-\alpha\boldsymbol{S}^{\mathrm{T}}\boldsymbol{S}\|=\sqrt{\lambda_{\max}[(\boldsymbol{I}-\alpha\boldsymbol{S}^{\mathrm{T}}\boldsymbol{S})^{\mathrm{T}}(\boldsymbol{I}-\alpha\boldsymbol{S}^{\mathrm{T}}\boldsymbol{S})]}=\sqrt{\lambda_{\max}[(\boldsymbol{I}-\alpha\boldsymbol{S}^{\mathrm{T}}\boldsymbol{S})^2]} \tag{17}$$

where, $\lambda_{\max}[\cdot]$ is the maximum eigenvalue of $[\cdot]$.

Since $\boldsymbol{S}^{\mathrm{T}}\boldsymbol{S}$ is a symmetric nonnegative definite matrix and normally there may be matrix of unfilled rank, which makes part of the eigenvalues zero. Therefore, 1 should be included in the eigenvalues of $(\boldsymbol{I}-\alpha\boldsymbol{S}^{\mathrm{T}}\boldsymbol{S})^2$, so $\sqrt{\lambda_{\max}[(\boldsymbol{I}-\alpha\boldsymbol{S}^{\mathrm{T}}\boldsymbol{S})^2]}\geqslant1$. $\boldsymbol{R}$ is not the compression operator.

2.2 Analysis of the semi-convergence of Landweber method

It is the unfilled rank of $\boldsymbol{S}^{\mathrm{T}}\boldsymbol{S}$ that makes the Landweber method semi-convergent, and the unfilled rank of $\boldsymbol{S}^{\mathrm{T}}\boldsymbol{S}$ is caused by ECT sensor, that is, the available independent capacitance number (the dimension number of $\boldsymbol{\lambda}$) is less than the pixel number of reconstructed images (the dimension number of $\boldsymbol{g}$). In addition, the sensitivity matrix $\boldsymbol{S}$ is got by ignoring the soft field effect; it doesn't represent the real characteristics of sensitivity field. In the iteration process, the accumulated error and data noise are easy to increase gradually, which makes the image reconstruction iteration semi-convergent.

3 Design of full convergence Landweber image reconstruction algorithm

3.1 Improvement of Landweber method

To solve the semi-convergence problem of Landweber method, we need to first improve the operator $\boldsymbol{R}$ to a compression operator. A new operator $\boldsymbol{R}'$ is structured with symmetry and nonnegative definite property of $\boldsymbol{S}^{\mathrm{T}}\boldsymbol{S}$.

$$\boldsymbol{R}' = \beta(\boldsymbol{I} - \alpha\boldsymbol{S}^{\mathrm{T}}\boldsymbol{S}) \tag{18}$$

where, β is decided based on $\| \boldsymbol{R}' \| < 1$, here $\boldsymbol{R}'$ is a compression operator. When $\beta = 1$, $\boldsymbol{R}'$ is the general iterative operator in normal Landweber method, so $\beta \in (-1, 1)$; α is a parameter related to the sensitivity matrix and ECT sensor systematic noise, and it can be used to control the iteration step size, generally, $0 < \alpha < \dfrac{2}{\lambda_{\max}(\boldsymbol{S}^{\mathrm{T}}\boldsymbol{S})}$.

Apply the improved iteration operator $\boldsymbol{R}'$ into Eq. (11),

$$\boldsymbol{g}_{k+1} = (\boldsymbol{I} + \boldsymbol{R}' + \cdots + \boldsymbol{R}'^{k})\boldsymbol{A}_0\boldsymbol{\lambda} \tag{19}$$

According to Eq. (9), Eq. (19) can be rewritten as

$$\boldsymbol{g}_{k+1} = \frac{\boldsymbol{I} - \boldsymbol{R}'^{k+1}}{\boldsymbol{I} - \boldsymbol{R}'}\boldsymbol{A}_0\boldsymbol{\lambda} \tag{20}$$

Take Eq. (20) as the iterative formula of Landweber algorithm after the improvement of the iteration operator, under the guarantee of correct choice of parameter, $\boldsymbol{R}'$ is the compression operator, the reconstructed image sequence will converge to $\dfrac{\boldsymbol{I}}{\boldsymbol{I} - \boldsymbol{R}'}\boldsymbol{A}_0\boldsymbol{\lambda}$.

3.2 The iteration stopping criterions based on a priori condition

Take Eq. (20) as the iterative formula of Landweber algorithm, the acquired image sequence $\{\boldsymbol{g}_k\}$ is mathematically convergent, but the limit of the image sequence may not be the actual permittivity distribution vector due to the defects of Eq. (4). Therefore, it is necessary to set a stopping iteration to guarantee the iteration stop when the iteration result is the closest to the real permittivity vector.

Define the priori condition $\Delta\boldsymbol{\lambda}$ as the error produced by sensitivity matrix in the process of mapping real permittivity distribution vector $\bar{\boldsymbol{g}}$ into capacitance vector,

$$\Delta\boldsymbol{\lambda} = \boldsymbol{\lambda} - \boldsymbol{S}\cdot\bar{\boldsymbol{g}} \tag{21}$$

The priori condition $\Delta\boldsymbol{\lambda}$ for different flow regimes (different projection $\boldsymbol{\lambda}$) is different. Use the least squares support vector machine (LS-SVM) classifiers to train a certain amount of classic image samples and predict the $\Delta\boldsymbol{\lambda}$ of the image.

If the image sample number is n, the independent capacitance number of ECT sensor is N, then LS-SVM training sample set can be described as $\{\boldsymbol{\lambda}_i, \Delta\lambda_i\}$ ($i = 1, 2, \cdots n$), where, $\boldsymbol{\lambda}_i$ is N dimensions normalized capacitance vector ($\boldsymbol{\lambda}_i$ can be obtained by finite element method according to the medium distribution of the image samples), $\Delta\lambda_i$ is the vector norm of the priori condition, then $\Delta\boldsymbol{\lambda}_i \in \mathbf{R}$. According to LS-SVM theory, the decision function for predicting the priori condition $\Delta\boldsymbol{\lambda}$ can be determined as:

$$\| \Delta\boldsymbol{\lambda}(\boldsymbol{\lambda}) \| = \sum_{i=1}^{n} \boldsymbol{\delta} K(\boldsymbol{\lambda}, \boldsymbol{\lambda}_i) + b \tag{22}$$

where, $K(\boldsymbol{\lambda}, \boldsymbol{\lambda}_i)$ is kernel function which is the high dimensional space integral operator, and radial basis function is used in this paper. $\boldsymbol{\delta}$ is the support vector. b is regression parameter.

The expression of kernel function $K(\boldsymbol{\lambda}_1, \boldsymbol{\lambda}_2)$ is shown as follow.

$$K(\boldsymbol{\lambda}_1, \boldsymbol{\lambda}_2) = \exp\left(-\frac{\| \boldsymbol{\lambda}_1 - \boldsymbol{\lambda}_2 \|}{\sigma^2}\right) \tag{23}$$

$\boldsymbol{\delta}$ and b can be obtained by solving the minimum equivalent value of LS-SVM method, which is described as follow.

$$\begin{bmatrix} 0 & 1 & 1 & \cdots & 1 \\ 1 & K(\boldsymbol{\lambda}_1, \boldsymbol{\lambda}_1) + \dfrac{1}{\gamma} & K(\boldsymbol{\lambda}_1, \boldsymbol{\lambda}_2) & \cdots & K(\boldsymbol{\lambda}_1, \boldsymbol{\lambda}_n) \\ 1 & K(\boldsymbol{\lambda}_2, \boldsymbol{\lambda}_1) & K(\boldsymbol{\lambda}_2, \boldsymbol{\lambda}_2) + \dfrac{1}{\gamma} & \cdots & K(\boldsymbol{\lambda}_2, \boldsymbol{\lambda}_n) \\ \vdots & \vdots & \vdots & & \vdots \\ 1 & K(\boldsymbol{\lambda}_n, \boldsymbol{\lambda}_1) & K(\boldsymbol{\lambda}_n, \boldsymbol{\lambda}_2) & \cdots & K(\boldsymbol{\lambda}_n, \boldsymbol{\lambda}_n) + \dfrac{1}{\gamma} \end{bmatrix} \cdot \begin{bmatrix} b \\ \delta_1 \\ \delta_2 \\ \vdots \\ \delta_n \end{bmatrix} = \begin{bmatrix} 0 \\ \Delta\lambda_1 \\ \Delta\lambda_2 \\ \vdots \\ \Delta\lambda_n \end{bmatrix} \tag{24}$$

σ and γ in Eq. (23) and (24) are respectively kernel parameter and regularization parameter; the values of both of them can be assigned according to experience.

The four flow regimes shown in Tab. 2 No. a ~ d are all the patterns for two-phase flow. Taking these four

flow regimes as image samples, to improve the prediction accuracy, we choose 10 images of different sizes for each regime, 40 samples in all.

When $\| \Delta\boldsymbol{\lambda} \|$ is closest to $\| \boldsymbol{\lambda} - \boldsymbol{S} \cdot \boldsymbol{g}_k \|$, $\boldsymbol{g}_k$ is the optimal solution, this could be the criterion for stopping iteration, that is to say, when Eq. (23) holds, the result of the k^{th} iteration step is the optimal solution.

$$\| \Delta\boldsymbol{\lambda} \| - \| \boldsymbol{\lambda} - \boldsymbol{S} \cdot \boldsymbol{g}_{k+1} \| > \| \Delta\boldsymbol{\lambda} \| - \| \boldsymbol{\lambda} - \boldsymbol{S} \cdot \boldsymbol{g}_k \| \tag{25}$$

4 Simulation and analysis

A simulation experiment is made with an 8-electrode ECT system and the capacitance value is calculated by finite element method. The finite element mesh is dot matrix of pixel of the imaging area. Five images are tested, four of which are of the same type with flow regimes samples, but size of discrete phase. The other flow regime is different from the samples at all points. For both traditional Landweber method and full-convergence Landweber method, iterate 100, 1 000 and 10 000 steps respectively, the image reconstruction resultsare shown in Tab. 2.

Comparing the reconstruction results in Tab. 2, it could be seen that when the iteration times reach 10 000,

Tab. 2 Results of image reconstruction

No.	Prototype	Algorithm	Iteration times 100	1000	10000
a	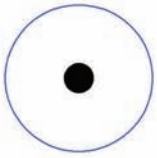	Landweber	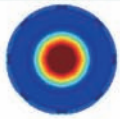	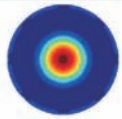	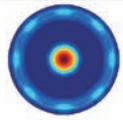
		Full-convergence Landweber	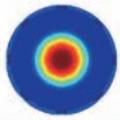		
b	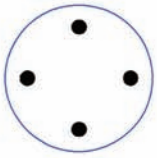	Landweber	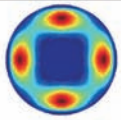	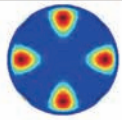	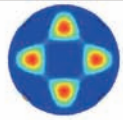
		Full-convergence Landweber	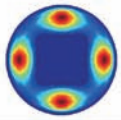	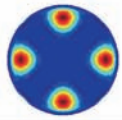	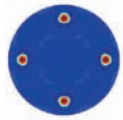
c	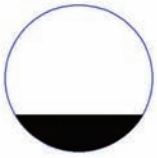	Landweber	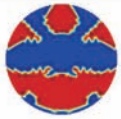	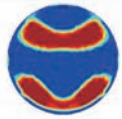	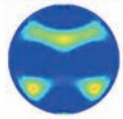
		Full-convergence Landweber	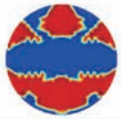		
d		Landweber	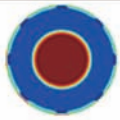	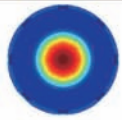	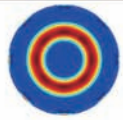
		Full-convergence Landweber	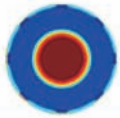	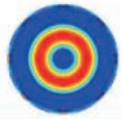	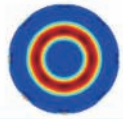
e	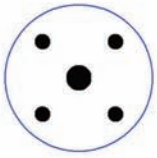	Landweber	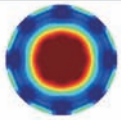	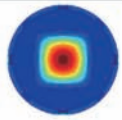	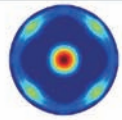
		Full-convergence Landweber	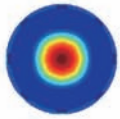	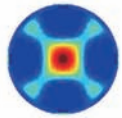	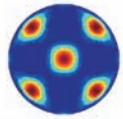

most image reconstruction results (except ring flow) of traditional Landweber method become obviously divergent. In fact, with more iteration times, the ring flow will be divergent too. However, the image reconstructions with full-convergence method are convergent stably, and the convergence rate is faster. For the flow pattern No. e in the Tab. 2 which is not shown in the samples, the reconstruction results with full-convergence are still convergent stably. In addition, it could be seen that the iteration times for different flow regimes are different. For the full-convergence Landweber algorithm, if Eq. (25) is used as iteration stopping criterions, the iteration will be stopped when the image is the relative optimum. Actually, by simulation, it can be found the full-convergence Landweber method can ensure that the final iteration result is the best one currently.

In Tabs. 3 and 4, we present the capacitance residuals and image relative error respectively (the items in these two tables are in accordance with those in Tab. 2). The calculation formulas are shown as follows:

$$\varepsilon_c = \frac{\| \boldsymbol{\lambda} - \boldsymbol{S} \cdot \hat{\boldsymbol{g}} \|}{\| \boldsymbol{\lambda} \|} \tag{26}$$

$$\varepsilon_i = \frac{\| \hat{\boldsymbol{g}} - \boldsymbol{g} \|}{\| \boldsymbol{g} \|} \tag{27}$$

where, $\hat{\boldsymbol{g}}$ is the permittivity distribution vector obtained from the image reconstruction algorithm.

Tab. 3 Capacitance residuals

No.	Algorithm	Iteration times		
		100	1 000	10 000
a	Landweber	0. 060 2	0. 052 6	0. 074 1
	Full-convergence Landweber	0. 054 9	0. 037 3	0. 033 5
b	Landweber	0. 073 3	0. 048 5	0. 038 6
	Full-convergence Landweber r	0. 064 9	0. 041 2	0. 030 6
c	Landweber	0. 434 7	0. 277 3	0. 256 1
	Full-convergence Landweber	0. 485 2	0. 251 6	0. 094 5
d	Landweber	0. 410 5	0. 253 0	0. 056 1
	Full-convergence Landweber	0. 399 2	0. 163 6	0. 052 7
e	Landweber	0. 433 0	0. 360 9	0. 078 6
	Full-convergence Landweber	0. 319 4	0. 291 8	0. 041 1

It can be concluded from Tab. 3 that for the sensitivity field (Nos. b, c and d in Tab. 2) whose sensitivity matrix $\boldsymbol{S}$ are varied a lot because of the different low regimes, when the reconstructed images with Landweber method become divergent, the capacitance residuals are still decreasing. It occurs because the sensitivity matrix $\boldsymbol{S}$ can't reflect the sensitivity field distribution accurately; therefore, the capacitance residuals cannot be regarded as image quality evaluation criteria and iteration stopping criteria. The problem can be solved by the method we proposed. It could be concluded from Tab. 4 that with the same iteration times, the full-convergence Landweber method has better image reconstruction accuracy than traditional Landweber method. According to Tab. 4, with a few iterations, the full-convergence Landweber method is not necessarily better than the original method. However, when a sufficient number of iterations (for example 10 000 times), the full-convergence Landweber can improve the accuracy of image by 16% ~ 50%, compared with Landweber. Therefore, in the multiphase flow measurement with less demanding real-time, the full-convergence Landweber can achieve higher detection accuracy.

Tab. 4 Image relative error %

No.	Algorithm	Iteration times		
		100	1 000	10 000
a	Landweber	43. 2	38. 3	49. 6
	Full-convergence Landweber	41. 5	36. 0	20. 1
b	Landweber	45. 2	39. 6	56. 3
	Full-convergence Landweber	41. 9	35. 4	22. 8
c	Landweber	55. 6	46. 7	54. 9
	Full-convergence Landweber	57. 3	47. 1	32. 4
d	Landweber	45. 8	42. 2	21. 0
	Full-convergence Landweber	45. 6	30. 9	20. 4
e	Landweber	60. 7	50. 6	31. 5
	Full-convergence Landweber	49. 2	33. 4	26. 1

5 Conclusions

A mathematical and physical analysis and demonstration of the semi-convergence of traditional Landweber method was made, and the inherent defects of image reconstruction with sensitivity matrix have been explored. The Landweber method is improved by structuring a compression operator to have full convergence characteristics. Meanwhile, a priori condition is applied to build an iteration stopping criteria, and thus corrects the effect of the structured compression operator on the convergence of Landweber method and compensates the deviation caused by sensitivity matrix. In practical application, the improved method can be self-adaptive and realize

optimal iteration steps. The simulation experiment shows that full-convergence Landweber method is more stable in convergence and higher in image reconstruction accuracy than traditional Landweber method.

References

[1] ZHANG Jingping, ZHU Jianxi, SUN Teng. Detection of apples' internal quality using CT imaging technology and Fourier transform[J]. Transactions of the Chinese Society for Agricultural Machinery, 2014, 45(5): 197 – 204. (in Chinese)

[2] YANG W Q. Design of electrical capacitance tomography sensors[J]. Measurement Science and Technology, 2010, 21(4): 1 – 13.

[3] YANG Y J, PENG L H. Data pattern with ECT sensor and its impact on image reconstruction[J]. IEEE Sensors Journal, 2013, 13(5): 1582 – 1593.

[4] WANG A N, MARASHDEH Q, FAN L S. ECVT imaging and model analysis of the liquid distribution inside a horizontally installed passive cyclonic gas-liquid separator[J]. Chemical Engineering Science, 2016, 141: 231 – 239.

[5] YE J M. Image filtering with associative Markov networks for ECT with distinctive phase origins[J]. IEEE Sensors Journal, 2012, 12(7): 2435 – 2443.

[6] XIE C G, HUANG S M, HOYLE B S, et al. Electrical capacitance tomography for flow imaging: system model for development of image reconstruction algorithm and design of primary sensor[J]. IEE Proceedings G-Circuits, Devices and System, 1992, 139(1): 89 – 98.

[7] YANG W Q, SPINK D M, York T A, et al. An image reconstruction algorithm based on Landweber's iteration method for electrical tomography[J]. Measurement Science and Technology, 1999, 10(11): 1065 – 1069.

[8] SOLEIMANI M, LIOHEART W R B. Nonlinear image reconstruction for electrical capacitance tomography using experimental data[J]. Measurement Science and Technology, 2005, 16(10):1987 – 1996.

[9] WANG Huaxiang, ZHU Xueming, ZHANG Lifeng. Conjugate gradient algorithm for electrical capacitance tomography[J]. Journal of Tianjin University, 2005, 38(1): 1 – 4. (in Chinese)

[10] YANG W Q, PENG L H. Image reconstruction algorithms for electrical capacitance tomography[J]. Measurement Science and Technology, 2003, 14(1): 1 – 13.

[11] LIU X, WANG X X, HU H L, et al. An extreme learning machine combined with Landweber iteration algorithm for the inverse problem of electrical capacitance tomography[J]. Flow Measurement and Instrumentation, 2015, 45(10): 348 – 356.

[12] CHEN Deyun, CHEN Yu, WANG Lili, et al. A novel Gauss – Newton image reconstruction for electrical capacitance tomography system[J]. Acta Electronica Sinica, 2009, 37(4): 739 – 743. (in Chinese)

[13] XIONG Xiaoyun, TANG Lei, WANG Chao. One-step stable image reconstruction algorithm for electrical capacitance tomo-graphy[J]. Chinese Journal of Science Instrument, 2007, 28(11): 1982 – 1986. (in Chinese)

[14] YAN H, WANG Y F, ZHOU Y G. Three-dimensional electrical capacitance tomography reconstruction by the Landweber iterative algorithm with fuzzy thresholding[J]. IET Science, Measurement and Technology, 2014, 8(6): 487 – 496.

[15] CHEN Yu, CHEN Deyun. Improved Runge – Kutta type Landweber image reconstruction algorithm for electrical capacitance tomography system[J]. Electric Machines and Control, 2014, 18(7): 107 – 112. (in Chinese)

[16] ZHANG L F. Landweber iteration algorithm based on sensitivity updating strategy for electrical capacitance tomography[J]. Journal of Chemical and Pharmaceutical Research, 2014, 6(2): 210 – 216.

[17] YE J M, WANG H G, LI Y, et al. Coupling of fluid field and electrostatic field for electrical capacitance tomography[J]. IEEEE Transactions on Instrumentation and Measurement, 2015, 64(12): 3334 – 3353.

[18] RAMLAU R, TESCHKE G, ZHARIY M. A compressive Landweber iteration for solving ill-posed inverse problem[J]. Inverse Problems, 2008, 24(6): 266 – 275.

[19] YANG Bin, YANG Xiaowei, HUANG Lan, et al. Adaptive and iterative algorithm of least square support vector machine regression[J]. Acta Electronica Sinica, 2010, 38(7): 1621 – 1625. (in Chinese)

[20] LI Y, YUAN X H, LIU J S, et al. An improved method of support vector machine algorithm with choosing segmentation in electrical capacitance tomography[J]. Information Technology Journal, 2013, 12(7): 1454 – 1458.

doi:10.6041/j.issn.1000-1298.2016.07.050

基于 ECT 图像重建算法的多相流检测研究

赵玉磊　郭宝龙

(西安电子科技大学空间科学与技术学院, 西安 710071)

摘要: 由于电容层析成像(ECT)图像重建的经典算法 Landweber 迭代法具有半收敛性,从而限制了其在多相流检测中的广泛应用。为了解决这一问题,从数学角度对 Landweber 法的半收敛性进行分析证明,并找到其物理本质原因。通过构造压缩算子提出一种全收敛的 Landweber 法,使得该方法具有稳定的收敛特性。同时,对 ECT 敏感场的"软场"特性进行分析,针对忽略"软场"特性所导致的经典 Landweber 法对不同流型的最佳迭代次数不一致的问题,利用最小二乘支持向量机对一定数量的图像样本进行训练,从而得到一个先验条件,并基于该先验条件提出一种自适应的迭代停止判据,实现在图像重建结果最接近多相流实际分布时停止迭代。仿真结果表明,改进后的方法不仅具有稳定收敛性,而且与 Landweber 法相比,图像重建精度可提高 16% ~50%。

关键词: 多相流; 检测; 图像重建; 电容层析成像; Landweber 法

中图分类号: TP274　　**文献标识码**: A　　**文章编号**: 1000-1298(2016)07-0368-07

Multiphase Flow Detection Based on ECT Image Reconstruction Algorithm

Zhao Yulei　Guo Baolong

(*School of Aerospace Science and Technology*, *Xidian University*, *Xi'an* 710071, *China*)

Abstract: Although Landweber method is a classical algorithm for image reconstruction in electrical capacitance tomography (ECT) system, the application of Landweber method in multiphase flow detection is limited due to its semi-convergence. To solve this problem, this paper analyzed and proved the semi-convergence of Landweber method mathematically so as to explore its physical properties. Based on this, an improved Landweber method with full and stable convergence was proposed by structuring a compression operator for Landweber. Then the "soft field" characteristic of sensitivity field in ECT sensor and its effect on sensitivity distribution, which is an important basis for image reconstruction, were analyzed. The sensitivity distributions for each typical electrode pair under different flow patterns were given in three-dimensional graphics. As ignoring "soft field" characteristic leads to inconsistency of the best iteration times of Landweber for different flow regimes, an adaptive iteration stopping criterion was proposed. The criterion is based on a priori condition obtained by training a number of image samples with least square support vector machine. With this criterion, iteration can be stopped when the image reconstructed is the closest to the actual distribution of multiphase flow. Meanwhile, the effect of "soft field" characteristic on image reconstruction could be compensated. The experimental results prove that the method not only has a stable convergence, but also can improve the image accuracy by 16% ~50%. Therefore, the full-convergence Landweber method can be widely used in none real-time multiphase flow measurement and detection system for its high detection precision.

Key words: multiphase flow; detection; image reconstruction; electrical capacitance tomography; Landweber method

收稿日期: 2016-01-03　修回日期: 2016-03-13

基金项目: 国家自然科学基金项目(61571346、61305041、61305040)和中央高校基本科研业务费专项资金项目(JB141305)

作者简介: 赵玉磊(1983—),男,博士生,主要从事多相流检测技术研究,E-mail: zhaoyulei_2008@aliyun.com

通信作者: 郭宝龙(1962—),男,教授,博士生导师,主要从事模式识别、神经网络与智能信息处理研究,E-mail: blguo@xidian.edu.cn

引言

农业生产领域中经常需要对多相流进行检测，如检测小麦与稻谷的含水率、牛奶的分相含率、土壤的盐碱度、食品检测[1]，以及对农机设备中输油管的无损检测。电容层析成像（Electrical capacitance tomography，ECT）是近年来出现的一种用于多相流浓度测量和可视化监测的技术，因其具有非侵入性、快速、低成本、无放射性等优点，被视为极具发展前景的过程层析成像技术[2-4]。

图像重建算法是 ECT 技术能否成功应用的重要因素，特别是农业生产中的多相流，其图像重建精度对检测结果具有至关重要的作用[5]。目前，ECT 图像重建的方法有线性反投影（Linear back-projection，LBP）法[6]、Landweber 法[7]、Tikhonov 正则化法[8]、Newton - Raphson 法以及共轭梯度（Conjugate gradient，CG）法[9]等。在这些图像重建方法中，以 LBP 法和 Landweber 法最具代表性，二者也是目前应用最广泛的 ECT 图像重建算法[10]。然而，LBP 法虽具有简单快速的优点，但其成像质量相对较差，严格讲，该方法仅是一种定性算法[4,10]；而 Landweber 法虽是最经典的图像重建迭代算法，其在 ECT 图像重建领域中也具有标杆性的地位[11]，但是由于 ECT 传感器敏感场的非线性及其“软场”特性的影响，又由于电容传感器的独立投影数据的数目（即独立电容值数目）小于重建图像的像素数[12]，使得 Landweber 法收敛到一定程度后，随着迭代次数的增加反而出现重建图像序列逐渐发散的情况，即半收敛[13-14]。此外，针对不同的流型，Landweber 法重建图像的收敛迭代次数也不一致，难以提出一个统一的判据作为其迭代停止条件。因此，在 Landweber 算法的基础上，提出一种改进方法，以解决其半收敛问题，并弥补 ECT“软场”特性造成的影响，对 ECT 技术在农业机械领域中的应用具有重要意义。

本文针对 Landweber 图像重建算法具有半收敛性这一问题，首先分析 ECT 敏感场的“软场”特性，以及用来描述敏感场的灵敏度矩阵对图像重建算法的影响；其次证明 Landweber 法的半收敛性，并分析其原因，从改进 Landweber 法的迭代算子和迭代停止判据两方面入手，提出一种改进方法，克服其半收敛性，实现重建图像的快速稳定收敛；最后给出图像重建的仿真结果，并与 Landweber 法进行比较。

1　ECT 敏感场特性分析及成像原理

1.1　ECT 的基本原理

ECT 技术的基本原理可以描述为：由于不同的介质具有不同的介电常数，若 2 种具有不同介电常数的物质混合在一起，则具有不同的混合物等价介电常数，当各物质组分浓度及（或）其分布发生变化时，该等价介电常数也会发生变化。该变化将反映为布置于多相流管道周围的阵列电极间的电容变化[10]。采用多电极阵列式电容传感器，其电极间的相互组合可提供反映多相流的相浓度与分布的多个电容测量值，以此作为投影数据，采用合适的图像重建算法，就可重建反映管道或装置在检测区域内的介质分布的图像。

ECT 系统由 3 个基本单元组成：电容传感器、测量与数据采集单元、图像重建计算机，如图 1 所示。

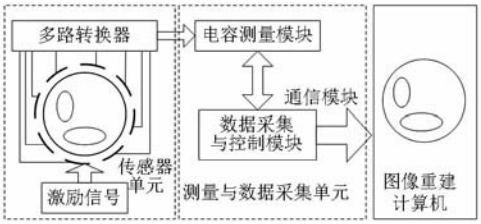

图 1　ECT 系统的组成结构

Fig. 1　Composition structure of ECT system

由于测量电路频率为 1 kHz 左右，传感器内的敏感场可看作是无自由电荷的静电场，可采用泊松方程描述为

$$\nabla(\varepsilon(x,y)\nabla\phi(x,y))=0 \tag{1}$$

式中　$\varepsilon(x,y)$——管道截面的介电常数分布

$\phi(x,y)$——管道截面的二维电势分布

∇——梯度算符

施加边界条件后，传感器不同电极组合之间的电容与敏感场中介电常数分布的关系可表示为[10]

$$C=\frac{Q}{V}=-\frac{1}{V}\iint_{\Gamma}\varepsilon(x,y)\nabla\phi(x,y)\,\mathrm{d}\Gamma \tag{2}$$

式中　Q——电容 C 所对应电极上的静电荷量

V——激励电压

Γ——电极所处的平面区域

若引入敏感场函数 $S(x,y,\varepsilon(x,y))$，则可将极板间电容 C 和 $\varepsilon(x,y)$ 的关系描述为

$$C=\iint_{D}\varepsilon(x,y)S(x,y,\varepsilon(x,y))\,\mathrm{d}x\mathrm{d}y \tag{3}$$

为简化问题，假定敏感场函数与 $\varepsilon(x,y)$ 无关，并将式(3)离散化、线性化和归一化为

$$\boldsymbol{\lambda}=\boldsymbol{S}\cdot\boldsymbol{g} \tag{4}$$

式中　$\boldsymbol{\lambda}$——归一化的实测电容向量，$\boldsymbol{\lambda}\in\mathbf{R}^m$

$\boldsymbol{S}$——归一化的灵敏度矩阵，$\boldsymbol{S}\in\mathbf{R}^{m\times n}$

$\boldsymbol{g}$——归一化的介电常数分布矢量，代表多相流的实际分布，$\boldsymbol{g}\in\mathbf{R}^n$[15]

ECT 图像重建就是通过测量电容得到介电常数分布，即由已知的 $\boldsymbol{\lambda}$ 求解未知量 $\boldsymbol{g}$。然而，由于未知量的个数（即像素数）远大于方程数（即测量电容个

数),因此式(4)为不定方程组,其解不唯一;同时,由于 ECT 传感器具有“软场”特性,其对图像重建影响极大。此外,式(4)还是一个病态方程,其解很不稳定[16]。因此,需要一个能够解决上述问题的 ECT 图像重建算法。

1.2 ECT 的“软场”特性

不同于 X 射线和 γ 射线形成的硬场,ECT 传感器中的敏感场具有“软场”特性。所谓“软场”,是指场域的灵敏度分布是不均匀的,并且灵敏度分布受到场中介质分布与异相介质的电容率差值的影响。“软场”特性是由电介质在电场中的极化现象引起的,因为电介质在极化作用下会产生束缚电荷,束缚电荷所产生的电场改变了原有静电场的分布[17]。

在“软场”特性的影响下,对应于不同的电介质及其分布,灵敏度分布具有很大差别。而在场域中介电常数分布未知的情况下,其灵敏度分布也不得而知,因此只能利用空场下的灵敏度分布进行图像重建。这就对图像重建造成极大影响。

本文以 8 电极 ECT 传感器的空场、泡流、环流和层流为例(介质成分为汽油和水),说明 ECT 场域的灵敏度分布特性。将传感器中的任意一个电极作为激励电极,并设为 1 号电极,其余电极顺次标记为 2~8 号,则不同电极对的敏感度分布如表 1 所示。从表中可以看出,在不同流型下,相同电极对间的灵敏度分布有较大差异,而灵敏度是静电场分布(电力线和等势面)的综合反映。所以,不同的流型(甚至是不同的介质成份)将对静电场分布产生直接影响,进而影响图像重建结果。

表 1 不同流型下的灵敏度分布

Tab. 1 Sensitivity distribution under different flow regimes

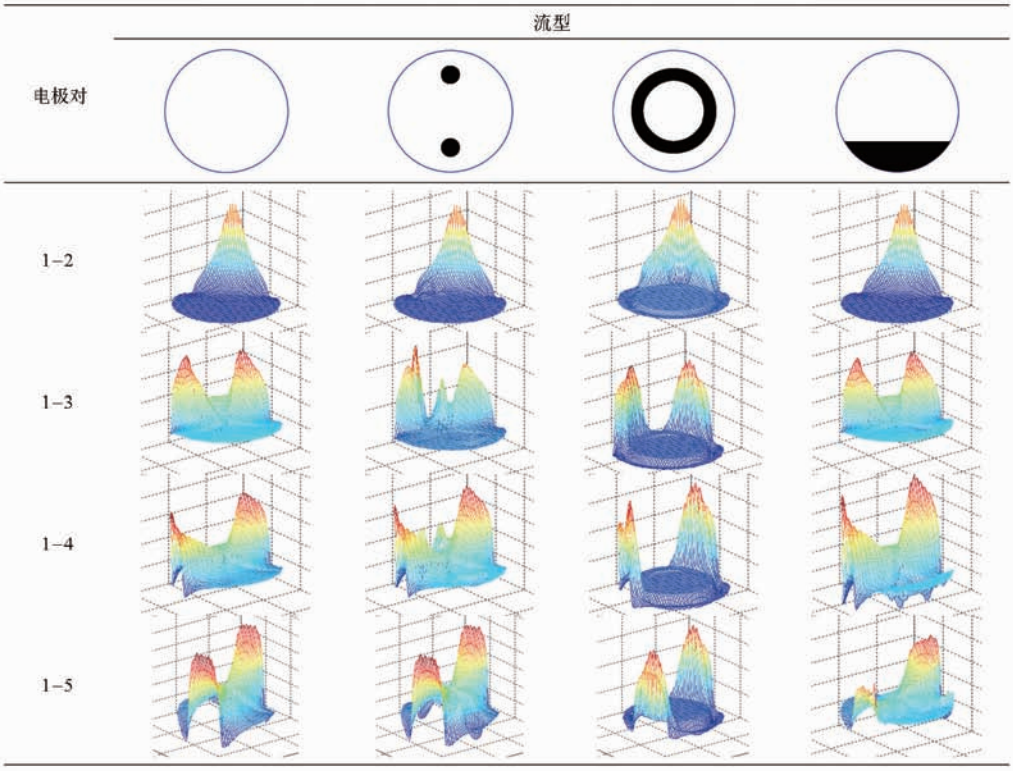

2 Landweber 法半收敛性的证明与分析

2.1 Landweber 法半收敛性证明

虽然 Landweber 法是目前最成熟的 ECT 图像重建算法,但其半收敛性却是该算法的缺陷,这也限制了 Landweber 算法的进一步推广。本文从级数理论的角度对其半收敛性进行推导证明。事实上,Landweber 图像重建算法的提出者,也正是利用级数对该方法进行数学解释的。

对于如式(4)所示的线性矩阵,假设 $\boldsymbol{A}_0$ 为 $\boldsymbol{S}^{-1}$ 的初始逼近矩阵,设 $\boldsymbol{I}$ 为单位阵,则存在残差矩阵

$$\boldsymbol{R} = \boldsymbol{I} - \boldsymbol{A}_0\boldsymbol{S} \tag{5}$$

若 $\boldsymbol{S}^{-1}$ 存在,可将式(5)写为

$$\boldsymbol{S}^{-1} = (\boldsymbol{I} - \boldsymbol{R})^{-1}\boldsymbol{A}_0 \tag{6}$$

如果残差 $\boldsymbol{R}$ 的谱半径 $\rho(\boldsymbol{R}) < 1$,则可将 $(\boldsymbol{I} - \boldsymbol{R})^{-1}$ 级数展开,且 $\boldsymbol{S}^{-1}$ 的第 k 项级数 $\boldsymbol{A}_k$ 和第 $k+1$ 项级数 $\boldsymbol{A}_{k+1}$ 分别为

$$\boldsymbol{A}_k = (\boldsymbol{I} + \boldsymbol{R} + \cdots + \boldsymbol{R}^{k-1})\boldsymbol{A}_0 \tag{7}$$

$$\boldsymbol{A}_{k+1} = (\boldsymbol{I} + \boldsymbol{R} + \cdots + \boldsymbol{R}^{k})\boldsymbol{A}_0 \tag{8}$$

又因为

$$(\boldsymbol{I} - \boldsymbol{R})(\boldsymbol{I} + \boldsymbol{R} + \cdots + \boldsymbol{R}^{k-1}) = \boldsymbol{I} - \boldsymbol{R}^k \tag{9}$$

根据式(5)、(7)、(9),可得到

$$\boldsymbol{R}^k\boldsymbol{A}_0=\boldsymbol{A}_0(\boldsymbol{I}-\boldsymbol{S}\boldsymbol{A}_k) \tag{10}$$

以第 $k+1$ 项级数 $\boldsymbol{A}_{k+1}$ 取代 $\boldsymbol{S}^{-1}$，并结合式(8)则有

$$\boldsymbol{g}_{k+1}=\boldsymbol{g}_k+\boldsymbol{R}^k\boldsymbol{A}_0\boldsymbol{\lambda} \tag{11}$$

再将式(10)代入式(11)可得到

$$\boldsymbol{g}_{k+1}=\boldsymbol{g}_k+\boldsymbol{A}_0(\boldsymbol{\lambda}-\boldsymbol{S}\boldsymbol{g}_k) \tag{12}$$

若令 $\boldsymbol{A}_0=\alpha\boldsymbol{S}^{\mathrm{T}}$，则式(12)可改写为

$$\boldsymbol{g}_{k+1}=\boldsymbol{g}_k+\alpha\boldsymbol{S}^{\mathrm{T}}(\boldsymbol{\lambda}-\boldsymbol{S}\boldsymbol{g}_k) \tag{13}$$

式中　α——增益因子，用以控制收敛速度[7]

式(13)就是 Landweber 法的一般迭代公式。

如前所述，仅当残差 $\boldsymbol{R}$ 的谱半径 $\rho(\boldsymbol{R})<1$ 时，才可保证式(13)成立，即级数收敛。因此，按照级数理论，Landweber 法的全收敛条件是 $\rho(\boldsymbol{R})=\|\boldsymbol{R}\|_2<1$，而算子 $\boldsymbol{R}$ 的范数可以定义为

$$\|\boldsymbol{R}\|=\max\frac{\|\boldsymbol{R}\boldsymbol{g}\|}{\|\boldsymbol{g}\|}\quad(\forall\boldsymbol{g}\in\mathbf{R}^n\text{ 且 }\boldsymbol{g}\neq0) \tag{14}$$

设 $\boldsymbol{g}=\boldsymbol{x}-\boldsymbol{y}$，任意 $\boldsymbol{x}$、$\boldsymbol{y}\in\mathbf{R}^n$，且 $\boldsymbol{x}\neq\boldsymbol{y}$，则有

$$\|\boldsymbol{R}\|\geqslant\frac{\|\boldsymbol{R}(\boldsymbol{x}-\boldsymbol{y})\|}{\|\boldsymbol{x}-\boldsymbol{y}\|} \tag{15}$$

即　　$$\|\boldsymbol{R}\boldsymbol{x}-\boldsymbol{R}\boldsymbol{y}\|\leqslant\|\boldsymbol{R}\|\cdot\|\boldsymbol{x}-\boldsymbol{y}\| \tag{16}$$

若 $\|\boldsymbol{R}\|<1$，则 $\boldsymbol{R}$ 为压缩算子，此时满足全收敛条件，所以 Landweber 法的全收敛条件是 $\boldsymbol{R}$ 为压缩算子。

以 2-范数为例，讨论 $\|\boldsymbol{R}\|$ 的特性。根据式(5)和 2-范数的数学定义，有

$$\|\boldsymbol{R}\|_2=\|\boldsymbol{I}-\alpha\boldsymbol{S}^{\mathrm{T}}\boldsymbol{S}\|=\sqrt{\lambda_{\max}[(\boldsymbol{I}-\alpha\boldsymbol{S}^{\mathrm{T}}\boldsymbol{S})^2]} \tag{17}$$

式中　$\lambda_{\max}[\cdot]$——矩阵$[\cdot]$的最大特征值

由于 $\boldsymbol{S}^{\mathrm{T}}\boldsymbol{S}$ 是一个对称、非负定的矩阵，并且通常不满秩[18]，这就造成其部分特征值为零，所以$(\boldsymbol{I}-\alpha\boldsymbol{S}^{\mathrm{T}}\boldsymbol{S})^2$ 的特征值包含 1。因此，$\sqrt{\lambda_{\max}[(\boldsymbol{I}-\alpha\boldsymbol{S}^{\mathrm{T}}\boldsymbol{S})^2]}\geqslant1$。故 $\boldsymbol{R}$ 通常不是压缩算子。

2.2　Landweber 法半收敛性的原因分析

Landweber 法半收敛性的直接原因是 $\boldsymbol{S}^{\mathrm{T}}\boldsymbol{S}$ 的不满秩，而造成 $\boldsymbol{S}^{\mathrm{T}}\boldsymbol{S}$ 不满秩的根本原因是在 ECT 传感器中，可得到的独立电容值的数目(即 $\boldsymbol{\lambda}$ 的维数)小于重建图像的像素数(即 $\boldsymbol{g}$ 的维数)。此外，由于灵敏度矩阵 $\boldsymbol{S}$ 是忽略“软场”效应后得到的，不能完全反映敏感场的特性，因此，在迭代的过程中，很容易使得累积误差和数据噪声逐步放大，也会造成图像重建迭代出现半收敛性[16]。

3　全收敛 Landweber 图像重建算法设计

3.1　Landweber 方法的改进

为了解决 Landweber 法的半收敛问题，需要对算子 $\boldsymbol{R}$ 进行改进，使其成为压缩算子。利用 $\boldsymbol{S}^{\mathrm{T}}\boldsymbol{S}$ 的对称性与非负定性，构造新的算子 $\boldsymbol{R}'$。

$$\boldsymbol{R}'=\beta(\boldsymbol{I}-\alpha\boldsymbol{S}^{\mathrm{T}}\boldsymbol{S}) \tag{18}$$

式中，β 的选择依据是使得 $\|\boldsymbol{R}'\|<1$，此时 $\boldsymbol{R}'$为压缩算子。当 $\beta=1$ 时，$\boldsymbol{R}'$就是一般 Landweber 方法的迭代算子，所以 $\beta\in(-1,1)$；α 是与灵敏度矩阵和 ECT 传感器系统噪声有关的参数，同时起到控制迭代步长的作用，一般可取 $0<\alpha<\dfrac{2}{\lambda_{\max}(\boldsymbol{S}^{\mathrm{T}}\boldsymbol{S})}$。

根据式(11)，应用改进后的迭代算子 $\boldsymbol{R}'$，有

$$\boldsymbol{g}_{k+1}=(\boldsymbol{I}+\boldsymbol{R}'+\cdots+\boldsymbol{R}'^k)\boldsymbol{A}_0\boldsymbol{\lambda} \tag{19}$$

结合式(9)可将式(19)改写为[13]

$$\boldsymbol{g}_{k+1}=\frac{\boldsymbol{I}-\boldsymbol{R}'^{k+1}}{\boldsymbol{I}-\boldsymbol{R}'}\boldsymbol{A}_0\boldsymbol{\lambda} \tag{20}$$

将式(20)视为改进迭代算子后的 Landweber 算法迭代格式。根据参数 β 的选择依据，$\boldsymbol{R}'$必为压缩算子，故由式(20)产生的重建图像序列是收敛的，其将收敛于$\dfrac{\boldsymbol{I}}{\boldsymbol{I}-\boldsymbol{R}'}\boldsymbol{A}_0\boldsymbol{\lambda}$。

3.2　基于先验条件的迭代终止判据

以式(20)作为 Landweber 方法的迭代格式，其所获得的图像序列$\{\boldsymbol{g}_k\}$，虽然在数学上是收敛的，但由于式(4)的近似性，并不能保证图像序列的极限就是实际的电容率分布矢量。因此，必须对迭代停止条件做出规定，以保证迭代结果在最逼近真实的电容率矢量时停止迭代。

定义先验条件 $\Delta\boldsymbol{\lambda}$ 为灵敏度矩阵将实际的电容率分布矢量 $\overline{\boldsymbol{g}}$ 映射为电容矢量时产生的误差，即

$$\Delta\boldsymbol{\lambda}=\boldsymbol{\lambda}-\boldsymbol{S}\cdot\overline{\boldsymbol{g}} \tag{21}$$

不同流型(即不同的投影 $\boldsymbol{\lambda}$)所对应的先验条件 $\Delta\boldsymbol{\lambda}$ 是不同的，采用最小二乘支持向量机(LS－SVM)分类方法，对一定数量的典型图像样本进行训练，从而预测出待测图像的 $\Delta\boldsymbol{\lambda}$。

若图像样本的数量为 n，ECT 传感器的独立电容数为 N，则可将 LS－SVM 的训练样本集表示为$\{\boldsymbol{\lambda}_i,\Delta\lambda_i\}(i=1,2,\cdots,n)$，其中，$\boldsymbol{\lambda}_i$ 为 N 维归一化的电容矢量($\boldsymbol{\lambda}_i$ 可根据所设图像样本的介质分布通过有限单元法求得)，$\Delta\lambda_i$ 为先验条件的向量范数，$\Delta\lambda_i\in\mathbf{R}$。由 LS－SVM 的理论，可确定用以预测先验条件 $\Delta\boldsymbol{\lambda}$ 的决策函数为

$$\|\Delta\boldsymbol{\lambda}(\boldsymbol{\lambda})\|=\sum_{i=1}^{n}\boldsymbol{\delta}K(\boldsymbol{\lambda},\boldsymbol{\lambda}_i)+b \tag{22}$$

式中　$K(\boldsymbol{\lambda},\boldsymbol{\lambda}_i)$——核函数[19]，为高维空间的内积，本文采用径向基函数

$\boldsymbol{\delta}$——支持向量

b——回归参数

核函数 $K(\boldsymbol{\lambda}_1,\boldsymbol{\lambda}_2)$ 计算式为

$$K(\boldsymbol{\lambda}_1,\boldsymbol{\lambda}_2)=\exp\left(-\frac{\|\boldsymbol{\lambda}_1-\boldsymbol{\lambda}_2\|}{\sigma^2}\right) \tag{23}$$

$\boldsymbol{\delta}$ 和 b 可通过求解与 LS-SVM 方法等效的最小值问题来获得[20],即

$$\begin{bmatrix} 0 & 1 & 1 & \cdots & 1 \\ 1 & K(\boldsymbol{\lambda}_1,\boldsymbol{\lambda}_1)+\dfrac{1}{\gamma} & K(\boldsymbol{\lambda}_1,\boldsymbol{\lambda}_2) & \cdots & K(\boldsymbol{\lambda}_1,\boldsymbol{\lambda}_n) \\ 1 & K(\boldsymbol{\lambda}_2,\boldsymbol{\lambda}_1) & K(\boldsymbol{\lambda}_2,\boldsymbol{\lambda}_2)+\dfrac{1}{\gamma} & \cdots & K(\boldsymbol{\lambda}_2,\boldsymbol{\lambda}_n) \\ \vdots & \vdots & \vdots & & \vdots \\ 1 & K(\boldsymbol{\lambda}_n,\boldsymbol{\lambda}_1) & K(\boldsymbol{\lambda}_n,\boldsymbol{\lambda}_2) & \cdots & K(\boldsymbol{\lambda}_n,\boldsymbol{\lambda}_n)+\dfrac{1}{\gamma} \end{bmatrix} \begin{bmatrix} b \\ \delta_1 \\ \delta_2 \\ \vdots \\ \delta_n \end{bmatrix} = \begin{bmatrix} 0 \\ \Delta\lambda_1 \\ \Delta\lambda_2 \\ \vdots \\ \Delta\lambda_n \end{bmatrix} \tag{24}$$

式(23)与式(24)中的 σ、γ 分别为核参数和正则化参数,二者可按经验取值。

选择如表 2 中序号 a ~ d 所示的 4 类流型作为图像样本,这4类流型基本包含了二相流的所有流

表 2 图像重建结果

Tab. 2 Results of image reconstruction

序号	流型	算法	迭代次数 100	迭代次数 1000	迭代次数 10000
a	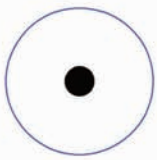	Landweber	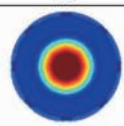	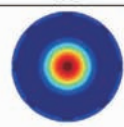	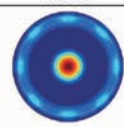
		全收敛 Landweber	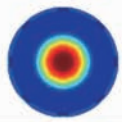		
b	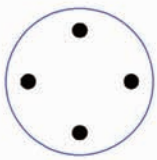	Landweber	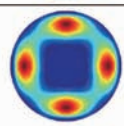	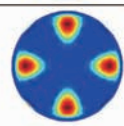	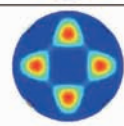
		全收敛 Landweber	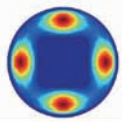	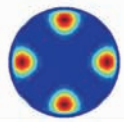	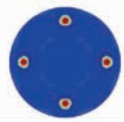
c	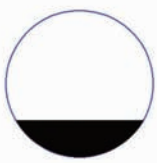	Landweber	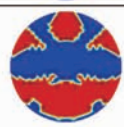	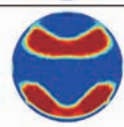	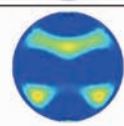
		全收敛 Landweber	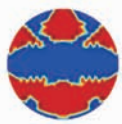		
d		Landweber	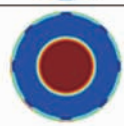	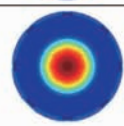	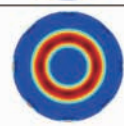
		全收敛 Landweber			
e	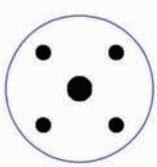	Landweber	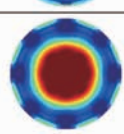	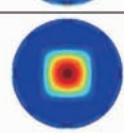	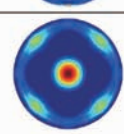
		全收敛 Landweber	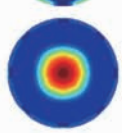	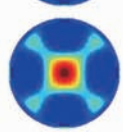	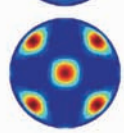

型种类。为了提高预测准确性，每类流型包括 10 个尺寸不同的图像，共计 40 个图像样本。

当 $\|\Delta\boldsymbol{\lambda}\|$ 与 $\|\boldsymbol{\lambda}-\boldsymbol{S}\cdot\boldsymbol{g}_k\|$ 最接近时，$\boldsymbol{g}_k$ 为最优解，因此可将该条件作为迭代的停止判据，即

$$\|\Delta\boldsymbol{\lambda}\|-\|\boldsymbol{\lambda}-\boldsymbol{S}\cdot\boldsymbol{g}_{k+1}\|>\|\Delta\boldsymbol{\lambda}\|-\|\boldsymbol{\lambda}-\boldsymbol{S}\cdot\boldsymbol{g}_k\| \tag{25}$$

若式(25)成立，则第 k 步的迭代结果就是最优解。

4　仿真分析

利用 8 电极 ECT 系统进行仿真，采用有限单元法计算测量电容值，并将有限元剖分网格作为成像区域的像素点阵。对 5 个流型分布图像进行仿真，其中 4 个是与图像样本同类的流型(流型尺寸与样本不同)，另一个流型与样本完全不同。将 Landweber 法和全收敛 Landweber 法分别迭代 100、1 000、10 000 次，对比其图像重建结果，如表 2 所示。由图像重建结果可以看出，Landweber 法对于除环流之外的流型，当迭代次数达到10 000次时，重建图像呈现出明显的发散性，事实上，对于环流，当迭代到一定次数时，Landweber 法的重建图像也会发散(本文中提到的发散是指随着迭代的进行，重建图像精度越来越低)。而全收敛 Landweber 法则呈现出稳定的收敛性，并且比 Landweber 法具有更快的收敛速度。对于未在图像样本中出现的流型(表 2 中序号 e)，全收敛 Landweber 法仍然表现出稳定的收敛性。此外，还可看出，对于不同的流型，Landweber 法的最优迭代次数并不一致；而对于全收敛 Landweber 法，以式(25)作为迭代停止依据，可以在图像相对最优时停止迭代。事实上，通过仿真发现，全收敛 Landweber 法可以保证最后一次迭代结果是当前最优的图像。

表 3、4 分别是 2 种方法重建图像的电容残差 ε_c 与相对图像误差 ε_i(表中的序号与表 2 中的序号相对应)，其计算公式分别为

$$\varepsilon_c=\frac{\|\boldsymbol{\lambda}-\boldsymbol{S}\cdot\hat{\boldsymbol{g}}\|}{\|\boldsymbol{\lambda}\|} \tag{26}$$

$$\varepsilon_i=\frac{\|\hat{\boldsymbol{g}}-\boldsymbol{g}\|}{\|\boldsymbol{g}\|} \tag{27}$$

式中　$\hat{\boldsymbol{g}}$——由图像重建算法得到的电容率分布矢量

由表 3 可以看出，对于因流型分布而使得灵敏度矩阵 $\boldsymbol{S}$ 改变较大的敏感场(表 2 中流型 b、c、e)，当 Landweber 法重建的图像已经发散时，但其电容残差仍在减小，这正是灵敏度矩阵 $\boldsymbol{S}$ 无法准确反映敏感场分布所造成的，因此将电容残差作为评价图像质量的指标并没有实际意义。同时也说明无法采用电容残差作为Landweber法的迭代停止依据，而采用本文提出的迭代停止判据，可以很好地解决这一问题。由表 4 可以看出，当迭代次数较少时，全收敛 Landweber 法不一定能够比 Landweber 法更优，但在迭代次数足够多的情况下(10 000 次)，全收敛 Landweber 法与经典 Landweber 法相比，图像精度可提高 16% ~ 50%，因此在对实时性要求不高的多相流检测中，全收敛 Landweber 法可达到更高的检测精度。

表 3　电容残差

Tab. 3　Capacitance residuals

序号	算法	迭代次数		
		100	1 000	10 000
a	Landweber	0.060 2	0.052 6	0.074 1
	全收敛 Landweber	0.054 9	0.037 3	0.033 5
b	Landweber	0.073 3	0.048 5	0.038 6
	全收敛 Landweber	0.064 9	0.041 2	0.030 6
c	Landweber	0.434 7	0.277 3	0.256 1
	全收敛 Landweber	0.485 2	0.251 6	0.094 5
d	Landweber	0.410 5	0.253 0	0.056 1
	全收敛 Landweber	0.399 2	0.163 6	0.052 7
e	Landweber	0.433 0	0.360 9	0.078 6
	全收敛 Landweber	0.319 4	0.291 8	0.041 1

表 4　图像相对误差

Tab. 4　Image relative error　%

序号	算法	迭代次数		
		100	1 000	10 000
a	Landweber	43.2	38.3	49.6
	全收敛 Landweber	41.5	36.0	20.1
b	Landweber	45.2	39.6	56.3
	全收敛 Landweber	41.9	35.4	22.8
c	Landweber	55.6	46.7	54.9
	全收敛 Landweber	57.3	47.1	32.4
d	Landweber	45.8	42.2	21.0
	全收敛 Landweber	45.6	30.9	20.4
e	Landweber	60.7	50.6	31.5
	全收敛 Landweber	49.2	33.4	26.1

5　结束语

分别从数学与物理的角度对 Landweber 图像重建方法的半收敛性进行分析证明，并找出利用灵敏度矩阵进行图像重建一系列方法的本质缺陷。在此基础上，通过构造一个压缩算子对 Landweber 法进行改进，使得改进后的方法基本具有全收敛的特性。同时，利用先验条件构造一个迭代停止判据，从而修正所构造的压缩算子对 Landweber 法迭代收敛性带来的影响，并补偿灵敏度矩阵造成的偏差，在实际应用中，可以实现自适应达到最佳迭代深度。仿真结果表明全收敛 Landweber 法较 Landweber 法具有更加稳定的收敛性，并具有更高的图像重建精度。

参 考 文 献

1 张京平, 朱建锡, 孙腾. 苹果内部品质的 CT 成像结合傅里叶变换方法检测[J]. 农业机械学报, 2014, 45(5): 197 - 204.
ZHANG Jingping, ZHU Jianxi, SUN Teng. Detection of apples' internal quality using CT imaging technology and Fourier transform [J]. Transactions of the Chinese Society for Agricultural Machinery, 2014, 45(5): 197 - 204. (in Chinese)

2 YANG W Q. Design of electrical capacitance tomography sensors[J]. Measurement Science and Technology, 2010, 21(4): 1 - 13.

3 YANG Y J, PENG L H. Data pattern with ECT sensor and its impact on image reconstruction[J]. IEEE Sensors Journal, 2013, 13(5): 1582 - 1593.

4 WANG A N, MARASHDEH Q, FAN L S. ECVT imaging and model analysis of the liquid distribution inside a horizontally installed passive cyclonic gas-liquid separator[J]. Chemical Engineering Science, 2016, 141: 231 - 239.

5 YE J M. Image filtering with associative Markov networks for ECT with distinctive phase origins[J]. IEEE Sensors Journal, 2012, 12(7): 2435 - 2443.

6 XIE C G, HUANG S M, HOYLE B S, et al. Electrical capacitance tomography for flow imaging: system model for development of image reconstruction algorithm and design of primary sensor[J]. IEE Proceedings G-Circuits, Devices and System, 1992, 139(1): 89 - 98.

7 YANG W Q, SPINK D M, York T A, et al. An image reconstruction algorithm based on Landweber's iteration method for electrical tomography[J]. Measurement Science and Technology, 1999, 10(11): 1065 - 1069.

8 SOLEIMANI M, LIOHEART W R B. Nonlinear image reconstruction for electrical capacitance tomography using experimental data [J]. Measurement Science and Technology, 2005, 16(10):1987 - 1996.

9 王化祥, 朱学明, 张立峰. 用于电容层析成像技术的共轭梯度算法[J]. 天津大学学报, 2005, 38(1): 1 - 4.
WANG Huaxiang, ZHU Xueming, ZHANG Lifeng. Conjugate gradient algorithm for electrical capacitance tomography[J]. Journal of Tianjin University, 2005, 38(1): 1 - 4. (in Chinese)

10 YANG W Q, PENG L H. Image reconstruction algorithms for electrical capacitance tomography[J]. Measurement Science and Technology, 2003, 14(1): 1 - 13.

11 LIU X, WANG X X, HU H L, et al. An extreme learning machine combined with Landweber iteration algorithm for the inverse problem of electrical capacitance tomography[J]. Flow Measurement and Instrumentation, 2015, 45(10): 348 - 356.

12 陈德运, 陈宇, 王莉莉, 等. 基于改进 Gauss - Newton 的电容层析成像图像重建算法[J]. 电子学报, 2009, 37(4): 739 - 743.
CHEN Deyun, CHEN Yu, WANG Lili, et al. A novel Gauss - Newton image reconstruction for electrical capacitance tomography system[J]. Acta Electronica Sinica, 2009, 37(4): 739 - 743. (in Chinese)

13 熊小芸, 唐磊, 王超. 用于电容层析成像的一步稳定图像重建算法[J]. 仪器仪表学报, 2007, 28(11): 1982 - 1986.
XIONG Xiaoyun, TANG Lei, WANG Chao. One-step stable image reconstruction algorithm for electrical capacitance tomo-graphy [J]. Chinese Journal of Science Instrument, 2007, 28(11): 1982 - 1986. (in Chinese)

14 YAN H, WANG Y F, ZHOU Y G. Three-dimensional electrical capacitance tomography reconstruction by the Landweber iterative algorithm with fuzzy thresholding[J]. IET Science, Measurement and Technology, 2014, 8(6): 487 - 496.

15 陈宇, 陈德运. 基于改进 Runge - Kutta 型 Landweber 的电容层析成像图像重建算法[J]. 电机与控制学报, 2014, 18(7): 107 - 112.
CHEN Yu, CHEN Deyun. Improved Runge - Kutta type Landweber image reconstruction algorithm for electrical capacitance tomography system[J]. Electric Machines and Control, 2014, 18(7): 107 - 112. (in Chinese)

16 ZHANG L F. Landweber iteration algorithm based on sensitivity updating strategy for electrical capacitance tomography[J]. Journal of Chemical and Pharmaceutical Research, 2014, 6(2): 210 - 216.

17 YE J M, WANG H G, LI Y, et al. Coupling of fluid field and electrostatic field for electrical capacitance tomography[J]. IEEEE Transactions on Instrumentation and Measurement, 2015, 64(12): 3334 - 3353.

18 RAMLAU R, TESCHKE G, ZHARIY M. A compressive Landweber iteration for solving ill-posed inverse problem[J]. Inverse Problems, 2008, 24(6): 266 - 275.

19 杨滨, 杨晓伟, 黄岚, 等. 自适应迭代最小二乘支持向量机回归算法[J]. 电子学报, 2010, 38(7): 1621 - 1625.
YANG Bin, YANG Xiaowei, HUANG Lan, et al. Adaptive and iterative algorithm of least square support vector machine regression[J]. Acta Electronica Sinica, 2010, 38(7): 1621 - 1625. (in Chinese)

20 LI Y, YUAN X H, LIU J S, et al. An improved method of support vector machine algorithm with choosing segmentation in electrical capacitance tomography[J]. Information Technology Journal, 2013, 12(7): 1454 - 1458.